





RESEARCH ARTICLE

Polyether-Derived Carbon Material and Ionic Liquid (Tributylmethylphosphonium iodide) Incorporated Poly(Vinylidene Fluoride-co-Hexafluoropropylene)-Based Polymer Electrolyte for Supercapacitor Application

Sehrish Nazir¹  | Pramod K. Singh¹  | Amrita Jain² | Monika Michalska³  | M. Z. A. Yahya⁴ | S. N. F. Yusuf⁵ | Markus Diantoro⁶ | Famiza Abdul Latif⁷ | Manoj K. Singh⁸ 

¹Center for Solar-Cells and Renewable Energy (CSRE), Department of Physics, SSBSR, Sharda University, Greater Noida, India | ²Institute of Fundamental Technological Research, Polish Academy of Sciences, Warsaw, Poland | ³Department of Chemistry and Physico-Chemical Processes, Faculty of Materials Science and Technology, VSB-Technical University of Ostrava, Ostrava, Czech Republic | ⁴Faculty of Defence Science and Technology, Universiti Pertahanan Nasional Malaysia (UPNM), Kuala Lumpur, Malaysia | ⁵Center for Ionics University of Malaya, Department of Physics, Faculty of Science, University of Malaya, Kuala Lumpur, Malaysia | ⁶Department of Physics, Faculty of Mathematics and Natural Science, Universitas Negeri Malang, Malang, Indonesia | ⁷Faculty of Applied Sciences, Universiti Teknologi MARA (Malaysia), Shah Alam, Malaysia | ⁸Energy Conversion & Storage Lab, Department of Applied Science and Humanities, Rajkiya Engineering College Banda, Uttar Pradesh, India

Correspondence: Sehrish Nazir (hsehrish471@gmail.com) | Pramod K. Singh (pramodkumar.singh@sharda.ac.in)

Received: 9 September 2024 | **Revised:** 25 September 2024 | **Accepted:** 19 October 2024

Funding: The authors received no specific funding for this work.

Keywords: capacitance | ionic conductivity | ionic liquid (IL) | solid polymer electrolyte (SPE) | supercapacitor (SC)

ABSTRACT

Poly(vinylidene fluoride-co-hexafluoropropylene) (PVdF-HFP)-sodium thiocyanate (NaSCN) solid polymer electrolytes containing different weight ratios of ionic liquid (IL)—tributylmethylphosphonium iodide (TBMPI) were prepared using solution-cast approach. Electrochemical impedance data indicates that increasing ionic liquid into polymer electrolyte matrix increases ionic conductivity and the maximum value of ionic conductivity was obtained at 150 wt% TBMPI, having conductivity value of $8.3 \times 10^{-5} \text{ S cm}^{-1}$. The dielectric measurement supports our conductivity data. Ionic transference number measurement affirms this system to be predominantly ionic in nature, while electrochemical stability window (ESW) was found to be 3.4 V. Polarized optical microscopy (POM) along with differential scanning calorimetry (DSC) suggest suitability of TBMPI as plasticizer, while infrared spectroscopy (FTIR) confirms ion interaction, complexation, and composite nature. The thermogravimetric analysis (TGA) shows thermal stability of these ionic liquid-doped polymer electrolytes (ILDPEs). Using maximum conducting ILDPE, a sandwiched supercapacitor has been fabricated which shows stable performance as high as 228 F g^{-1} using cyclic voltammetry (CV).

1 | Introduction

Energy storage is one of the major concerns arising in today's time. Environmental problems include the decreasing availability of energy sources such as fossil fuels and the enormous amount of greenhouse gas emissions produced as a consequence

of their increased overuse [1]. Interest in methods of storing energy as well as other forms of renewable energy has increased as a result of these issues [2, 3]. Compared to batteries, SCs offer an increased power density and an increased energy density than conventional capacitors, making them the forthcoming generations of devices for storing energy that are generating much

attention [4]. Supercapacitors are usually categorized into three types based on how they hold charge [5]. A pseudocapacitor is a first kind of capacitor that stores charge via faradaic reaction. The next type is known as an electrical double layer capacitor (EDLC), which functions by storing electrical energy on the space between the electrode and electrolyte by means of the reverse adsorption of ions. A hybrid capacitor, which was developed by integrating the technologies of EDLCs and pseudocapacitors, is the third kind of capacitor. Pseudocapacitors utilize rapid interface redox reactions to store energy, and their energy density becomes comparable to that of batteries when paired with nanostructured lithium electrodes. It is well documented that in EDLC, carbon serves as an electrode material, while as in pseudocapacitor, metal oxide frameworks and conducting polymers serve as electrode materials, and in hybrid capacitor, a mixture of carbon and molecular orbitals/charge carriers is utilized, and charge accumulation occurs through both Faradaic and non-Faradaic mechanisms [6]. Additionally, in EDLC, the charge-storing approach is facilitated by the development of an electrochemical double layer, which somewhat is a non-Faradaic phenomenon, while as in pseudocapacitor, the charge is accumulated via redox reactions, which involve the transfer of electrons (Faradaic process), and in hybrid capacitor, the charge accumulation occurs through both Faradaic and non-Faradaic mechanisms [7].

A supercapacitor is made up of two porous electrodes that are sandwiched together by an electrolyte that has an elevated ionic conductivity, excellent electrochemical window, and strong thermal and mechanical strength [8]. Supercapacitor is more environmentally friendly than batteries due to its higher power density, longer lifespan, and higher cyclability. Different electrodes, including graphite, carbon nanogel, activated carbon (AC), and carbon nanotubes (CNTs), have been used to study and create supercapacitors. Particularly in applications requiring low energy density, supercapacitor might be thought of as a good alternative to traditional batteries [9].

The reason solid polymer electrolyte (SPE) films are used in supercapacitor is because they don't require novel technologies, have a large working temperature range, reduced volatility, and an increased energy density and little to no vapor pressure [10]. Numerous studies on liquid electrolytes have found that they have good ionic conductivities but also have issues with handling, corrosion, leakage, and evaporation. Researchers discovered that solid polymer electrolytes (SPEs) have advantages over liquid electrolytes by resolving their drawbacks [11]. The formation of high ionic conducting solid polymer electrolytes (SPEs) for use in energy device applications is the main goal of polymer conducting research. The most popular electrochemical energy storage technologies include capacitors, fuel cells, and conventional batteries. The manufacture of supercapacitors using SPEs has received a great deal of attention in the literature. The research community has paid close attention to supercapacitors as an alternative energy storage method. Among other advantages over secondary batteries, supercapacitor has a longer cycle life (over 10^3 cycles), requires no maintenance, is devoid of harmful elements, has a higher power density, a larger capacitance, and discharges quickly [12]. Additionally, the electrode/electrolyte contact in EDLC stores the charge electrostatically, enabling the charging-discharging process to occur in a matter of seconds. Furthermore, compared to current liquid electrolytes, solid polymer electrolyte-based

supercapacitors offer the advantage of reducing leakages [13]. Solid polymer electrolytes can be used to get around the aforementioned issues. Ionic species that have been dissolved in a polymer host make up solid polymer electrolytes. Several distinct SPEs have been synthesized in the recent years using a range of host polymers, including poly(ethylene oxide), poly(vinyl alcohol), and polyvinylpyrrolidone (PVP), incorporated with various additives like ionic salts, plasticizers, and ILs. ILs are exclusively salts having melting points below 100°C , and they are molten salts at low temperatures or at room temperature. Due to their wide electrochemical potential window, thermal stability, minor volatility, nonflammability, and potential for a significant cation-anion combination, ILs have recently attracted interest.

Polymer electrolytes have utilized various host polymers, including poly(vinyl alcohol) (PVA), PEO [14], poly(vinyl pyrrolidone) (PVP), poly(vinylidene fluoride) (PVdF), poly(methyl methacrylate) (PMMA), poly(ethylmethacrylate) (PEMA), poly(acrylonitrile) (PAN), poly(vinylidene fluoride-co-hexafluoropropylene) (PVdF-HFP), and others [15].

PVdF-HFP is a copolymer that is formed through the process of copolymerization between PVdF and hexafluoropropylene (HFP) [16]. The mechanical strength and amorphous character of the co-polymer PVdF-HFP are enhanced through this procedure, resulting in improved qualities. The presence of the $(-\text{C}-\text{F})$ group in PVdF-HFP serves as an electron withdrawing group, enhancing the anodic stability [17]. The co-polymer PVdF-HFP exhibits significant solubility in organic solvents, resulting in reduced crystallinity compared to pure PVdF polymer due to a decrease in the glass transition temperature. The use of PVdF-HFP has the capacity to enhance the efficiency, safety, and longevity of energy storage devices [18], specifically supercapacitor [19]. Due to its versatile use as a binder, electrolyte additive, separator layer, and component of supercapacitors, this polymer holds significant value in the field of energy storage [20]. Numerous organic polymers have been employed in the production of carbon materials; however, there are no documented studies regarding the utilization of polyethylene oxide (PEO)-derived carbon and its application in supercapacitors. Consequently, PEO is more economical, and the yield of the final product (carbon material) is 40%, which is adequate for future energy uses [21].

In this paper, we have synthesized solid polymer electrolyte films using PVdF-HFP polymer, mixed with NaSCN salt and doped tributylmethylphosphonium iodide ionic liquid (IL) as plastisizer using solution-cast technique.

Finally, the electrochemical performance of fabricated supercapacitor sandwiched using maximum-conducting ILDPE as electrolyte and polyether-derived carbon-based electrodes is also given in detail.

2 | Experimental Section

2.1 | Materials

For the synthesis of solid polymer electrolyte films, we have used poly(vinylidene fluoride-co-hexafluoropropylene) (PVdF-HFP) as host polymer, sodium thiocyanate (NaSCN)

as ion-source, and ionic liquid—tributylmethylphosphonium iodide as plasticizer. PVdF-HFP was purchased from Sigma Aldrich (USA), having molecular weight (Mw): $4 \times 10^5 \text{ g mol}^{-1}$. NaSCN having molecular weight (Mw): 81.07 g mol^{-1} was purchased from Central Drug House, New Delhi (India). Ionic liquid—tributylmethylphosphonium iodide was also purchased from TCI Pvt. Ltd. (India). The current collector, that is, graphite sheet, was purchased from Nickunj Eximp Entp Pvt. Ltd., Mumbai, India.

2.2 | Synthesis of Polymer Electrolyte

The solution-cast technique was used to develop different polymer electrolyte films. The chosen adequate amounts of PVdF-HFP (Mw = $4 \times 10^5 \text{ g mol}^{-1}$) were dissolved in solvent (acetone). A fixed amount of 40 wt% of NaSCN was added to the solution and stirred for approximately 10 h until we obtained a viscous, transparent solution. The solution of PVdF-HFP and NaSCN was then doped with different amounts of IL ($x = 25, 50, 100, 150,$ and 200 wt\% of IL) and stirred overnight till homogenous solutions were obtained. The thick ILDPE solutions were then poured into various petri dishes and kept at room temperature for overnight to remove all the common solvent molecules.

2.3 | Synthesis of Carbon (Electrode Material)

In this work, carbon was synthesized using a polyether—polyethylene oxide (PEO)—reported by our group [21] to use it in electrodes for supercapacitor as an active material. Poly(ethylene oxide) (PEO) was carbonized in a tubular furnace under an inert atmosphere to yield pure carbon (non-porous carbon). The procedure involved gradually increasing the temperature of the PEO at a constant rate of $5^\circ\text{C}/\text{min}$ until it reached a temperature of 800°C . After reaching the desired temperature, the sample was kept on hold at 800°C for 30 min to confirm effective carbonization. After the specified duration, the sample was cooled down to the ambient temperature using a consistent pace of $5^\circ\text{C}/\text{min}$. By maintaining an inert environment throughout the process, oxidation was effectively prevented, thereby ensuring the purity of the carbon material. The progressive heating and cooling technique employed in this process successfully eliminated non-carbon components from PEO, yielding a pure carbon material with few structural defects. Once cooled, the material was crushed into a fine powder and then underwent a washing process. This involved first using a diluted hydrochloric acid (HCl) solution, followed by deionized water. At last, the carbon powder was subjected to an overnight drying process at around 100°C in a vacuum oven and thereafter preserved in an atmosphere free from reactive gases [22].

2.4 | Characterization of Polymer Electrolyte

The polymer electrolytes were analyzed using Electrochemical Impedance Spectroscopy (EIS), Ionic Transference Number (t_{ion}), Linear Sweep Voltammetry (LSV), Polarized Optical Microscopy (POM), Differential Scanning Calorimetry (DSC),

Thermogravimetric Analysis (TGA), and Fourier transform infrared (FTIR) to investigate their electrical, thermal, structural, and electrochemical properties.

2.5 | Fabrication of Supercapacitor

For the fabrication of supercapacitor, a slurry was prepared using the polyether-based carbon material, acetylene black, and PVdF-HFP as a binder. Here 10 wt% PVdF-HFP was dissolved in acetone by keeping the solution on a magnetic stirrer for 3–4 h. After that, 80 wt% carbon material and 10 wt% acetylene black were grinded in mortar and pestle, followed by the addition of PVdF-HFP solution (binder solution) dropwise to make a slurry. Lastly, the prepared slurry ($\sim 1 \text{ mg}$) was coated on each graphite sheet (current collector) of $1 \times 1 \text{ cm}^2$ area, and the prepared electrodes were kept in a vacuum oven at 80°C overnight for vacuum drying.

To assemble the supercapacitor, the optimized 150 wt% ionic liquid (TBMPI) incorporated PVdF-HFP conducting solid polymer electrolyte film was placed in between the prepared identical carbon electrodes (carbon-coated graphite sheets). Afterwards, the fabricated supercapacitor cell was placed within a sample holder to facilitate further electrochemical examination.

2.6 | Characterization of Supercapacitor

The fabricated cells were analyzed using cyclic voltammetry (CV) and low frequency impedance spectroscopy (LIS) techniques to examine their electrochemical properties, which include specific capacitance of the assembled supercapacitor.

3 | Results and Discussion

3.1 | Electrochemical Impedance Spectroscopy (EIS)

Prior to conducting EIS measurement, the thickness of each polymer electrolyte was measured using a screw gauge. The ILDPE films were subsequently exposed to electrochemical impedance spectroscopy (EIS) for measuring the ionic conductivity. The solid polymer electrolyte film was placed between two identical stainless-steel electrodes throughout the measurement. The impedance of polymer electrolyte films was assessed using CH Instrument Electrochemical Workstation (model 604D, USA). The ionic conductivity of each solid polymer electrolyte was measured using the following equation:

$$\sigma = \frac{l}{R_b A} \quad (1)$$

The symbol “ σ ” denotes the ionic conductivity, measured in S cm^{-1} . The variable “ l ” represents the thickness of the polymer film, measured in cm. “ R_b ” represents the bulk resistance of the polymer electrolytes, measured in Ω . The value of “ R_b ” was obtained from the Nyquist plot, whereas “ A ” represents the surface

area of the probe under which the sample is placed, measured in square centimeters (cm²).

Bulk resistance “ R_b ” is a significant factor in determining the conductivity of an electrolyte system. Based on the real (Z') and imaginary (Z'') values of impedance, we have evaluated the value of “ R_b ” as shown in Figure 1. These evaluated values were then put in Equation (1) to obtain the conductivity values. The calculated values are reported in Table 1 and displayed in Figure 2.

It is clear that by incorporating various weight percentages (wt%) of TBMPI into the polymer matrix, the initial ionic conductivity experiences a rapid increase, reaching maxima at 150 wt% with conductivity value $8.3 \times 10^{-5} \text{ Scm}^{-1}$, after which it decreases. The increase in ionic conductivity is attributed to the increase in the quantity of mobile charge carriers or ease of ion movement within the electrolyte (reduced crystallinity). Conversely, the decrease in conductivity is caused by the ion-pair formation within the matrix, a phenomenon extensively documented in literature [23–25]. Furthermore, after 200 wt% IL concentration, we experienced difficulty in taking out the SPE freestanding film from the petri dish. Therefore, all measurements were conducted up to 200 wt% IL.

3.1.1 | Dielectric Constant

Figure 3 illustrates the relationship between the dielectric constant and the concentration of ionic liquid (IL) in the PVdF-HFP: NaSCN polymer salt complex. The initially noticed rise in the dielectric constant is caused by an increase in the number of charge carriers. The dielectric constant further increases as a result of increased mobility. The little reduction in dielectric constant can be attributed to the rise in ion clusters within IL-incorporated polymer electrolyte, resulting in a reduction in conductivity. The dielectric constant and conductivity of the polymer matrix are significantly affected by the concentrations of ionic charges. Furthermore, it can be noted that the dielectric

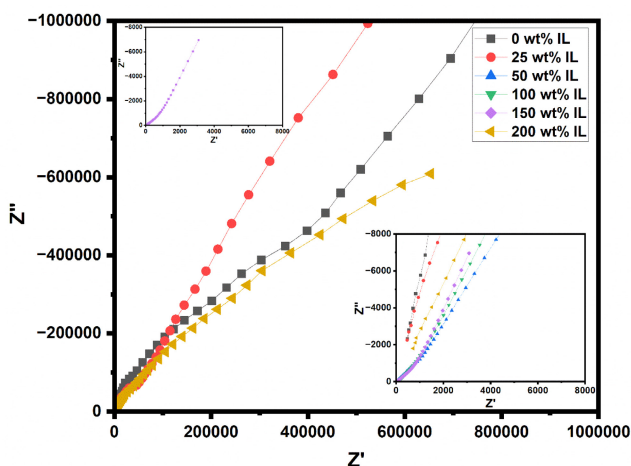


FIGURE 1 | Impedance spectra for polymer electrolyte (PVdF-HFP + 40 wt% NaSCN) along with different IL-incorporated polymer electrolyte films, insight plots of the maximum conductivity film, and magnified graphs of all the mentioned compositions.

constant and mobility exhibit a similar pattern, as depicted in Figure 2 and Table 2.

3.2 | Ionic Transference Number (t_{ion})

Measuring the ionic transport number is a crucial technique for determining the individual contributions of ionic and electronic conductivity to the overall electrical conductivity of materials. The transference number is defined as the ratio of the electric current generated by the cation to the overall electric current. If the transference number approaches 1, it indicates that the dominant factor contributing to the ion conduction in the polymer electrolyte is the cation. A high transference number can decrease the concentration polarization of electrolytes during charge–discharge cycles, resulting in increased power density.

The ionic transference number in the Wagner's polarization approach can be determined using Equation (2).

$$t_{ion} = \frac{\text{initial current} - \text{final current}}{\text{initial current}} \quad (2)$$

To evaluate t_{ion} of one typical ILDPE film, an electric potential of 500 mV is applied over the maximum conductive polymer electrolyte film that is set between two stainless-steel electrodes for a duration of 1 h approximately. Time v/s current plot was recorded using CH instrument Electrochemical Workstation (model 604D, USA). Ultimately, the t_{ion} value is ascertained by referring to Figure 4 and is determined to be 0.95. This finding indicates that the primary constituent of the electrolyte is predominantly composed of ions only. We have measured t_{ion} value of various ILDPE films, and their value is more than 0.90, which shows that these ILDPE systems are predominantly ionic in nature.

3.3 | Linear Sweep Voltammetry (LSV)

The CH Instruments Electrochemical Workstation (model 604D, USA) was used to assess the electrochemical characteristics, specifically the potential window of ILDPE polymer electrolytes.

The electrochemical stability window (ESW) of the most conductive electrolyte film was determined by LSV. To evaluate

TABLE 1 | Values of ionic conductivity calculated for various SPE films at ambient temperature.

Composition	Ionic conductivity (Scm^{-1})
[A]	7.3×10^{-8}
[A] + 25 wt% IL	6.6×10^{-7}
[A] + 50 wt% IL	3.3×10^{-5}
[A] + 100 wt% IL	5.2×10^{-5}
[A] + 150 wt% IL	8.3×10^{-5}
[A] + 200 wt% IL	1.7×10^{-6}

ESW of these ILDPes, a typical maximum conducting ILDP film was sandwiched between two stainless steel electrodes and applied voltage range from -3V to $+3\text{V}$, as shown in Figure 5. It is clear that the electrochemical stability window (ESW) of the ILDP system was 3.4V , which is reasonably good for application in electrochemical devices.

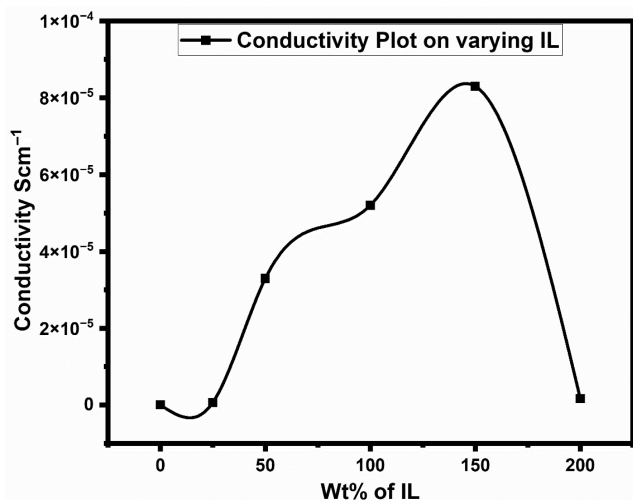


FIGURE 2 | Dependency of ionic conductivity in polymer electrolyte with variation in IL concentrations.

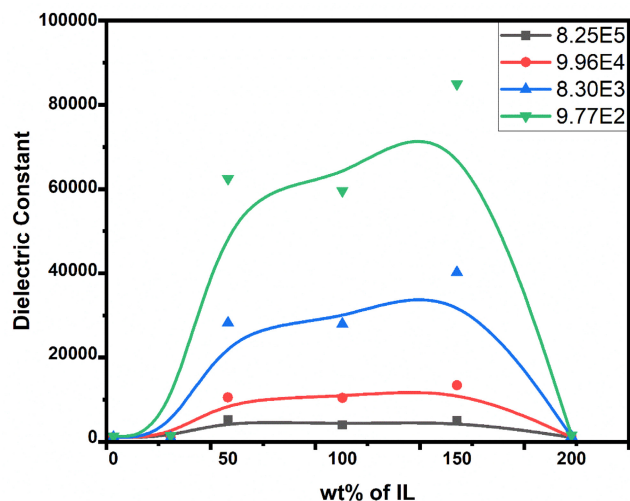


FIGURE 3 | The dielectric constant changes in polymer electrolyte systems with respect to IL content.

TABLE 2 | Dielectric constant values at various frequencies.

wt% of IL	$8.25 \times 10^5 \text{ Hz}$	$9.96 \times 10^4 \text{ Hz}$	$8.30 \times 10^3 \text{ Hz}$	$9.77 \times 10^2 \text{ Hz}$
0%	72	89	133	336
25%	75	96	22	445
50%	4277	9648	27493	62107
100%	3072	9556	27283	59194
150%	4105	12538	39642	84799
200%	93	139	289	666

3.4 | Polarized Optical Microscopy (POM)

Figure 6 illustrates the surface morphology of pure PVdF-HFP, PVdF-HFP: NaSCN polymer salt complex, and ionic liquid-incorporated polymer electrolyte films. (Figure 6a) clearly depicts the surface of the pure PVdF-HFP film, which appears solid and smooth with minimal radiant crystals, confirming its semi-crystalline nature. The polymer-salt complex film (Figure 6b) exhibits a reduction in crystallite size along with more dark patches, which indicate the decrease in crystalline matrix as a result of salt infiltrating the polymer matrix. In addition, the surface of the film becomes more darker when we added IL to polymer matrix, indicating a further reduction in crystalline regions.

3.5 | Differential Scanning Calorimetry (DSC)

The thermal characteristics of the SPE films formed were examined by the use of differential scanning calorimetry (DSC). Figure 7 displays the DSC curves for pristine PVdF-HFP, PVdF-HFP with 40wt% NaSCN, and PVdF-HFP with 40wt% NaSCN and 150wt% IL.

$$\chi_c = \frac{\Delta H_m}{\Delta H_m^0} \times 100 \quad (3)$$

The percentage of crystallinity has been determined by following Equation (3).

Where, ΔH_m is the melting enthalpy found experimentally and ΔH_m^0 is the referenced melting enthalpy for PVdF-HFP (i.e., 104.7 J g^{-1}) [26]. The obtained values of χ and ΔH_m are presented in Table 3.

It is clear that crystallinity goes down once we add salt (NaSCN) or IL in the polymer electrolyte (Table 3), which supports our observations observed in conductivity as well as POM.

3.6 | Thermogravimetric Analysis (TGA)

To evaluate the thermal stability of the prepared SPEs, thermogravimetric analysis (TGA) was performed. This was done by observing the change in weight of a sample while it was heated at a constant pace, as shown in Figure 8.

As per American Society for Testing and Materials (ASTM), thermal degradation is a technique, when the raised temperature on material, causes changes in mechanical, electrical, and physical properties. Thermal degradation is the molecular deterioration in polymers at elevated temperature. When a polymer

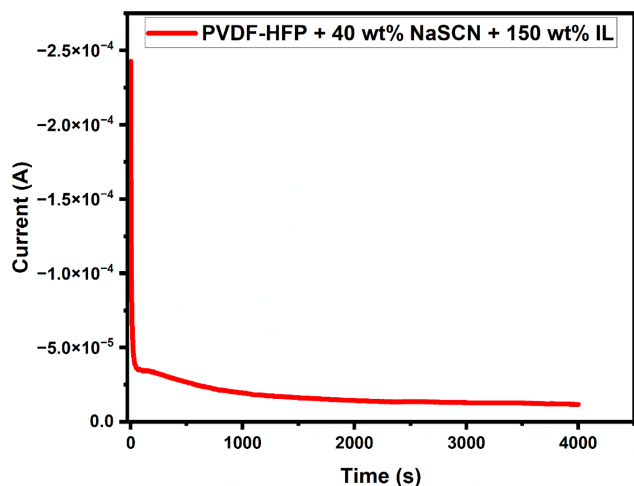


FIGURE 4 | Ionic transference of the maximum conducting polymer electrolyte film (PVdF-HFP + 40 wt% NaSCN + 150 wt% IL).

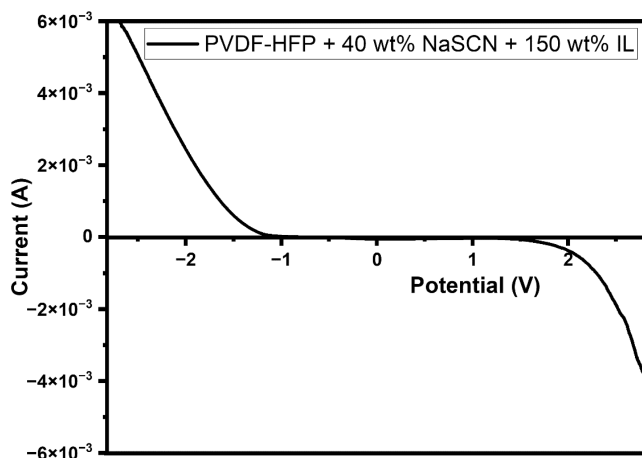


FIGURE 5 | LSV response of the maximum conducting polymer electrolyte film (PVdF-HFP + 40 wt% NaSCN + 150 wt% IL).

chain is subjected to excessive heat, its components undergo separation and react with each other, resulting in a modification of the properties of polymer. In general, this belongs to change in the polymer molecular weight. Typically, it can be concluded that changes include like chalking, cracking, ductility reduction, color changes, and reduction in the most other physical properties of polymer. Figure 8 depicts the TGA profile of prepared polymer electrolyte films, (a) pristine PVDF-HFP, (b) PVdF-HFP + NaSCN, and (c) PVdF-HFP + NaSCN + TBMPI films which exhibits the thermal stability of films before adding ionic species and after adding ionic species. From the figure, it is clearly observed that pure PVDF-HFP film was stable up to 436.84°C having the weight loss percent of material approximately 98%. After this instant, the film was degraded at very sharp rate, and the weight of PVDF-HFP becomes 25.06% at 504.33°C. Incorporation of salt (Figure 8b) curve shows the weight initially decreased sharply to 79.88% at a temperature of 99.95°C, which was caused by the presence of water molecules in the sample after adding NaSCN to the PVDF-HFP polymer film. After this point, the film was stable up to 394.35°C having weight 76.19%. Then at last, the film was degraded at a very fast rate, and the weight of material reaches 7.80% only at 775.56°C. Figure 8c, after adding IL, the same pattern was observed. Initial declination was observed due to presence of water molecules and then was stable up to 296.58°C, having weight of film 85.65%. Eventually, the film underwent rapid degradation and attained a weight of 13.38% at a temperature of 775.56°C. Thermal degradation of polymer after incorporating ion species is a more convoluted problem, where filler seriously affects the polymer stability. It is clearly seen from the TGA profile that after adding ion species NaSCN + TBMPI on a host polymer PVDF-HFP somehow the thermal stability temperature decreases and reaches approximately 300°C (Figure 8c), but still, to operate a device at ambient temperature, it could be a good sign to look for the future work using same polymer electrolyte to reach up to the industrial phase.

3.7 | Fourier Transform Infrared Spectroscopy (FTIR)

FTIR spectroscopy is used to analyze the synthesized samples and investigate the interactions between IL, salt, and polymer. This analysis helps determine the presence of various chemical

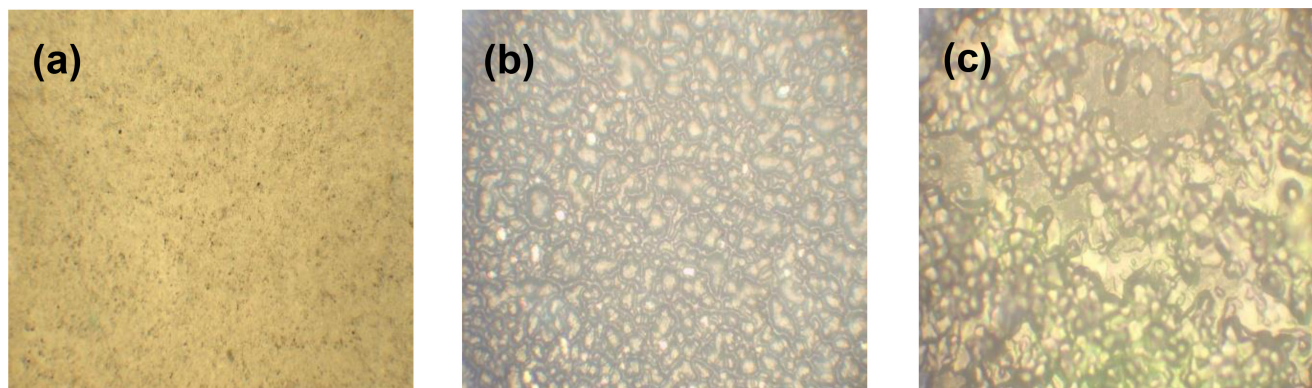


FIGURE 6 | Optical micrographs for (a) pristine PVdF-HFP, (b) PVdF-HFP with NaSCN, and (c) PVdF-HFP with NaSCN and TBMPI at 10× magnifications.

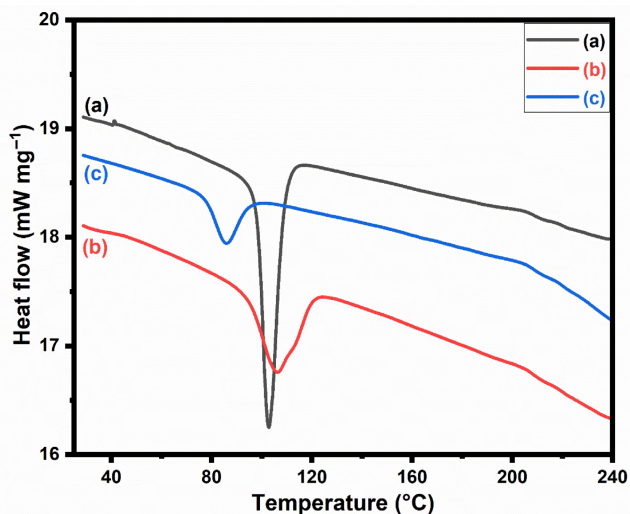


FIGURE 7 | DSC curves for (a) PVdF-HFP, (b) PVdF-HFP + 40wt% NaSCN, and (c) PVdF-HFP + 40wt% NaSCN + 150wt% IL.

TABLE 3 | Melting enthalpy (ΔH_m) and relative percentage of crystallinity (χ) of (a) pristine PVdF-HFP, (b) PVdF-HFP + 40wt% NaSCN, and (c) PVdF-HFP + 40wt% NaSCN + 150wt% IL.

Composition	ΔH_m (J g ⁻¹)	χ (%)
PVdF-HFP	52.00	50
PVdF-HFP + 40wt% NaSCN	30.35	29
PVdF-HFP + 40wt% NaSCN + 150wt% IL	22.70	22

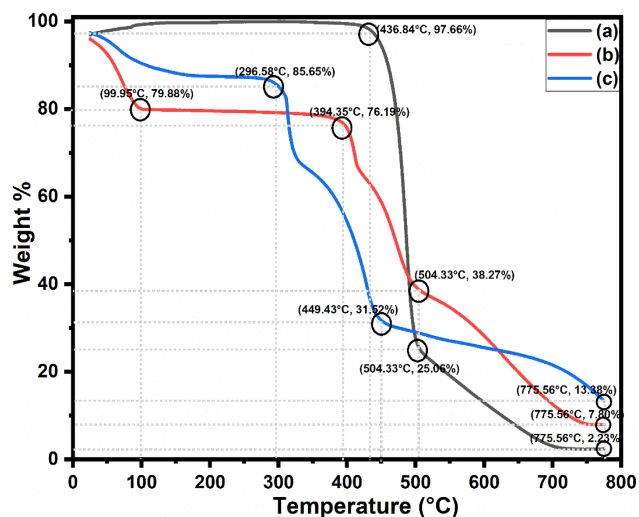


FIGURE 8 | TGA profile for (a) pristine PVdF-HFP, (b) PVdF-HFP + 40wt% NaSCN, and (c) PVdF-HFP + 40wt% NaSCN + 150wt% IL.

bonds and reactive functional groups. All polymer samples with FTIR spectra obtained between 4000 and 650 cm^{-1} are represented in Figure 9. Figure 9 displays the FTIR spectra of various substances: pure PVdF-HFP, pure salt (NaSCN), ionic liquid

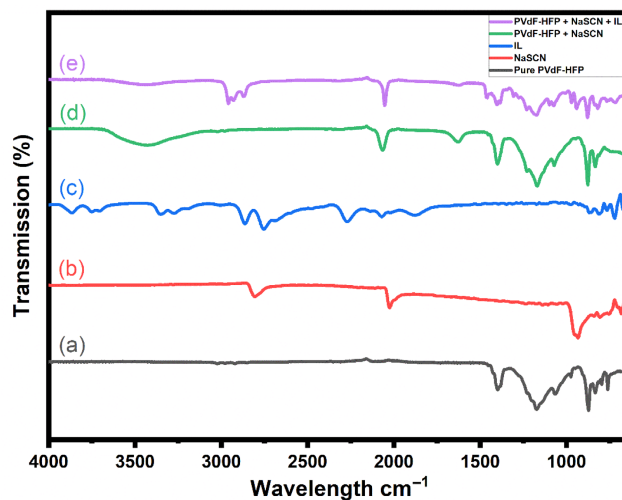


FIGURE 9 | FTIR spectroscopy of the prepared SPE samples: (a) Pure PVdF-HFP, (b) NaSCN, (c) IL, (d) PVdF-HFP + 40wt% NaSCN, and (e) PVdF-HFP + 40wt% NaSCN + 150wt% IL.

(TBMPI), polymer salt matrix PVdF-HFP: NaSCN, and a highly conducting SPE film incorporated with IL.

Figure 9 shows the FTIR spectra of pure PVdF-HFP, pure salt (NaSCN), ionic liquid (TBMPI), polymer-salt matrix PVdF-HFP: NaSCN, and greatest conducting SPE film incorporated with IL.

Figure 9a displays the infrared spectrum of pure PVdF-HFP. Peaks were detected at positions 1400, 1172, 1065, and 795 cm^{-1} . A vibrational S=O stretch detected at 1400 cm^{-1} indicates the existence of sulfate and sulfonyl chloride; O-H bending suggests the presence of carboxylic acid and alcohol, while the C-F stretch confirms the presence of fluoro compounds. Similarly, at other peaks like 1172, 1065, and 795 cm^{-1} , we can observe C-F stretching, C-N stretching, and C-O stretching at peak position 1172 cm^{-1} that confirms the presence of fluoro compound, amine, ester, and tertiary alcohol, groups respectively. At 1065 cm^{-1} , there is C-F stretching, C-N stretching, C-O stretching, and S=O stretching that affirm the presence of fluoro compound, amine, primary alcohol, and sulfoxide groups, respectively. We observed C-Cl stretching, C=C bending, and C-H bending at the peak position 795 cm^{-1} that suggests the existence of halo compound, alkene, 1,4-disubstituted, 1,2,3,4-tetrasubstituted, and 1,2,3-trisubstituted, respectively.

The NaSCN spectrum in Figure 9b exhibits prominent peaks at 3408, 2060, and 755 cm^{-1} , indicating the presence of alcohol, isothiocyanate, and halo compound groups corresponding to O-H stretching, N=C=S stretching and C-H bending, respectively. The existence of a carboxylic acid and alcohol group is indicated by a band of O-H stretching vibration noticed at 2957 cm^{-1} . Additionally, the occurrence of an alkane group is suggested by the peak location of bending vibration of C-H at 2872 cm^{-1} (Figure 9c). The stretching vibrations of O-H and N=C=S bonds are represented by two bands seen at 3432 and 2063 cm^{-1} (Figure 9d). The major peaks observed at 1398, 1167 and 874 cm^{-1} correspond to O-H bending that affirms the presence of carboxylic acid and alcohol groups, vibrations caused by

TABLE 4 | FTIR assessment for (a) Pure PVdF-HFP, (b) NaSCN, (c) IL (TBMPI), (d) PVdF-HFP+NaSCN, and (e) PVdF-HFP + NaSCN + IL (TBMPI).

Component	Wavenumber (cm ⁻¹)	Peak assignment	Class	References
PVdF-HFP	1400	O–H bending	Carboxylic acid	[28–30]
		O–H bending	Alcohol	
		S=O stretching	Sulfate	
		S=O stretching	Sulfonyl chloride	
		C–F stretching	Fluoro compound	
	1172	C–F stretching	Fluoro compound	[31–34]
		C–N stretching	Amine	
		C–O stretching	Ester	
	1065	C–O stretching	Tertiary alcohol	[35, 36]
		C–F stretching	Fluoro compound	
		C–N stretching	Amine	
		C–O stretching	Primary alcohol	
		S=O stretching	Sulfoxide	
	795	C–Cl stretching	Halo compound	[37, 38]
C=C bending		Alkene		
C–H bending		1,4-Disubstituted		
C–H bending		1,2,3,4-Tetrasubstituted		
C–H bending		1,2,3-Trisubstituted		
NaSCN	3408	O–H stretching	Alcohol	[39]
	2060	N=C=S stretching	Isothiocyanate	[40, 41]
	755	C–Cl stretching	Halo compound	[42]
C–H bending		1,2-Disubstituted		
IL (TBMPI)	2957	C–H bending	Monosubstituted	[27, 43]
		O–H stretching	Carboxylic acid	
		O–H stretching	Alcohol	
		N–H stretching	Amine salt	
	2872	C–H stretching	Alkane	[44, 45]
		O–H stretching	Carboxylic acid	
		O–H stretching	Alcohol	
	1460	N–H stretching	Amine salt	[46, 47]
		C–H stretching	Alkane	
	816	C–H bending	Alkane	[48, 49]
		C–Cl stretching	Halo compound	
C=C bending		Alkene		
C–H bending		1,4-Disubstituted		
C–H bending		1,2,3,4-Tetrasubstituted		

(Continues)

TABLE 4 | (Continued)

Component	Wavenumber (cm ⁻¹)	Peak assignment	Class	References
PVdF-HFP + NaSCN	3432	O–H stretching	Alcohol	[50]
	2063	N=C=S stretching	Isothiocyanate	[51]
	1626	C=C stretching	Alkene	[52–54]
		N–H bending	Amine	
	1398	O–H bending	Carboxylic acid	[26, 55]
		O–H bending	Alcohol	
		S=O stretching	Sulfate	
	1167	C–F stretching	Fluoro compound	
		C–F stretching	Fluoro compound	[56, 57]
		C–N stretching	Amine	
		C–O stretching	Ester	
		C–O stretching	Tertiary alcohol	
	874	C–H bending	1,2,4-Trisubstituted	[58]
		C–H bending	1,3-Disubstituted	
	831	C–Cl stretching	Halo compound	[59]
C=C bending		Alkene		
PVdF-HFP + NaSCN + IL (TBMPI)	2957	O–H stretching	Carboxylic acid	[27, 43, 60]
		O–H stretching	Alcohol	
		N–H stretching	Amine salt	
		C–H stretching	Alkane	
	2053	N=C=S stretching	Isothiocyanate	[37, 61]
	1402	C–H bending	Alkane	[62, 63]
		O–H bending	Carboxylic acid	
		O–H bending	Alcohol	
	1173	S=O stretching	Sulfate	
		S=O stretching	Sulfonyl chloride	
		C–F stretching	Fluoro compound	[62, 64]
		C–N stretching	Amine	
		C–O stretching	Ester	
	877	C–O stretching	Tertiary alcohol	
		C–H bending	1,2,4-Trisubstituted	[28, 65]
C–H bending		1,3-Disubstituted		
818	C–Cl stretching	Halo compound	[33, 66]	
	C=C bending	Alkene		
	C–H bending	1,4-Disubstituted		
	C–H bending	1,2,3,4-Tetrasubstituted		

the stretching of S=O indicate the existence of sulfate group and C–F stretching shows the presence of fluoro compound at peak position 1398 cm⁻¹. At 1167 cm⁻¹, we observed a band of C–F stretching, C–N stretching, and C–O stretching that suggest the

presence of fluoro compound, amine, ester, and tertiary alcohol groups, respectively. The strong peak position at 874 cm⁻¹ shows C–H bending that suggests the presence of 1,2,4-trisubstituted and 1,3-disubstituted functional groups.

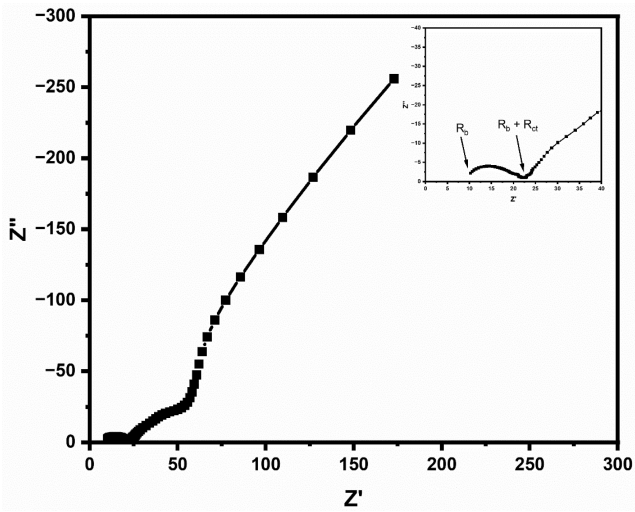


FIGURE 10 | Low-frequency impedance spectroscopy measurement conducted to determine the specific capacitance (C_{sp}) of the developed EDLC.

Typically, during the process of NaSCN salivation in PVdF-HFP, the Na^+ cations are confined within the spiral structure (called helix) of the PVdF-HFP chain, while the SCN^- anions are piled outside the spiral structure. The breakdown of the NaSCN lattice structure leads to changes in the SCN^- stretching modes due to ion interactions. The introduction of NaSCN to PVdF-HFP results in the emergence of three additional peaks in the FTIR spectrum at 3432, 2063, and 1626 cm^{-1} . These peaks signify a modification in the micro-structural and vibrational arrangement of the polymer salt matrix.

FTIR spectrum of ionic liquid-incorporated polymer electrolyte in Figure 9e shows various peaks at 2957, 2053, 1402, 1173, 877, and 818 cm^{-1} . The peak position 2957 cm^{-1} corresponds to stretching vibration of O–H, N–H, and C–H bonds and is assigned to carboxylic acid, alcohol, amine salt, and alkane, respectively. Another peak at 2053 cm^{-1} corresponding to stretching vibration of N=C=S shows the presence of isothiocyanate group. The band observed at 1402 cm^{-1} corresponds to the stretching vibration of C–H, O–H, and S=O bonds that

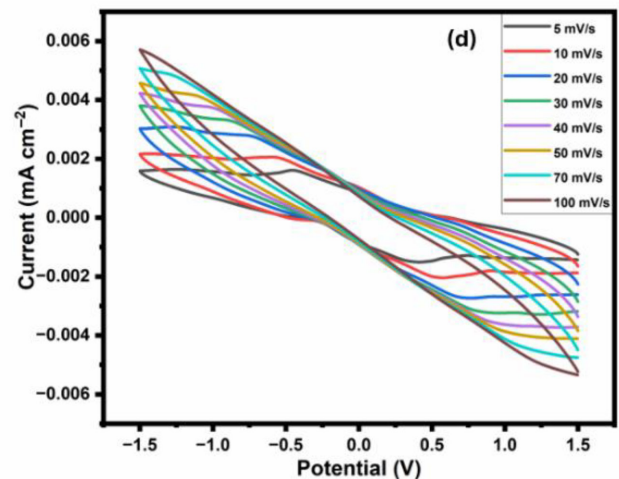
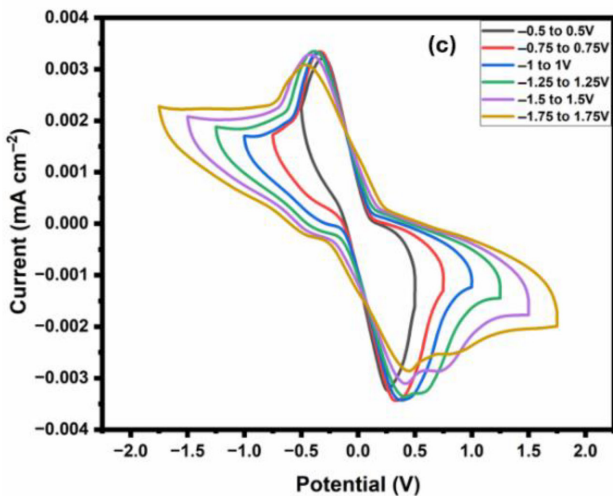
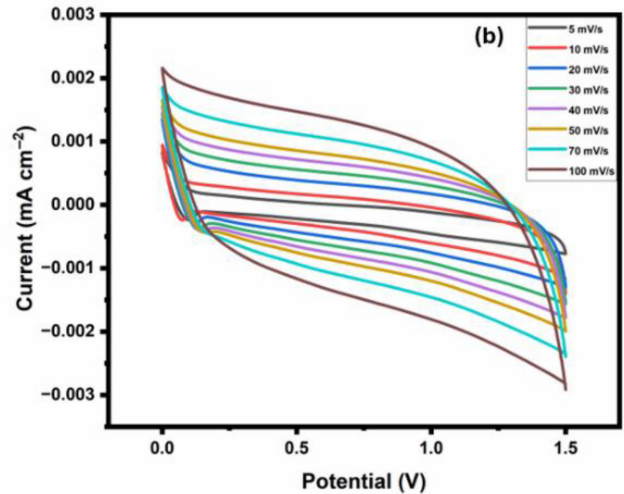
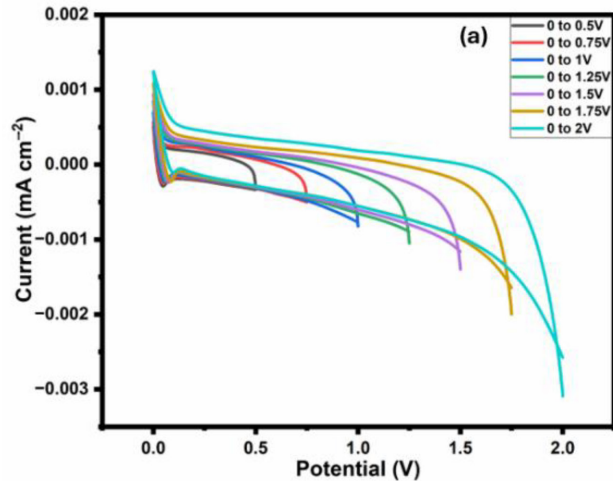


FIGURE 11 | CV-curve of the activated carbon and solid polymer electrolyte-based supercapacitor cell at (a) various voltage ranges starting from 0 to various positive values keeping scan rate 10 mVs^{-1} , (b) various scan rates keeping voltage range 0 to 1.5 V, (c) various voltage ranges starting from various negative to positive values keeping scan rate 10 mVs^{-1} , and (d) various scan rates keeping voltage range -1.5 to 1.5 V.

TABLE 5 | Specific capacitance of the supercapacitor cell at varied voltage ranges (0 to x V) with scan rate of 10 mVs^{-1} .

Voltage (V)	Specific capacitance (Fg^{-1})
0–0.5	37
0–0.75	39
0–1	41
0–1.25	46
0–1.5	49
0–1.75	59
0–2	74

TABLE 6 | Specific capacitance of the supercapacitor cell at varied scan rates (voltage range from 0 to 1.5).

Scan rate (mVs^{-1})	Specific capacitance (Fg^{-1})
5	60
10	49
20	41
30	36
40	33
50	30
70	27
100	23

TABLE 7 | Specific capacitance of the supercapacitor cell at varied voltage ranges ($-x$ to x V), with scan rate of 10 mVs^{-1} .

Voltage (V)	Specific capacitance (Fg^{-1})
–0.5 to 0.5	211
–0.75 to 0.75	211
–1 to 1	201
–1.25 to 1.25	205
–1.5 to 1.5	202
–1.75 to 1.75	199

suggest the existence of alkane, carboxylic acid, alcohol, sulfate, and sulfonyl chloride, respectively. Similarly, at other peaks like 1173 , 877 , and 818 cm^{-1} , we can observe C–F stretching, C–N stretching, and C–O stretching at peak position 1173 cm^{-1} that confirms the presence of fluoro compound, amine, ester, and tertiary alcohol groups, respectively. At 877 cm^{-1} , there is C–H bending that affirms the presence of 1,2,4-trisubstituted and 1,3-disubstituted functional groups. At 818 cm^{-1} peak position, we observed C–Cl stretching that suggests the presence of halo compound, C=C bending suggests the existence of alkene, and the bending vibration of C–H bonds suggests the presence of 1,4-disubstituted and 1,2,3,4-tetrasubstituted functional groups.

TABLE 8 | Specific capacitance of the supercapacitor cell at varied scan rates (voltage range from -1.5 to 1.5).

Scan rate (mVs^{-1})	Specific capacitance (Fg^{-1})
5	228
10	143
20	87
30	61
40	45
50	35
70	23
100	14

It is evident that the peak spots in the polymer salt matrix have altered when compared to pristine PVdF-HFP. There are no extra peaks observed, indicating that the salt ions have formed complexes with the functional groups of the polymer PVdF-HFP [27]. Figure 9e clearly demonstrates an evident shift in the peak positions of the infrared spectra of the polymer electrolyte system incorporated with ionic liquid (IL) compared to the polymer salt matrix. The IL-incorporated polymer electrolyte film has nearly all the characteristic peaks associated with PVdF-HFP, NaSCN, or IL, with a notable alteration in intensity. The text illustrates the interaction of salt cation and IL cation with the C–H and C–N stretching of the polymer PVdF-HFP. Nevertheless, the presence of high IL content has an impact on the structure of the polymer electrolyte due to the presence of large cations and reactive anions [SCN], as shown in Table 4.

From the above table, it can be observed that all the major peaks in the PVdF-HFP + NaSCN + TBMPI polymer electrolyte film are either from pure PVdF-HFP or NaSCN or ionic liquid (TBMPI); that means no new peaks are formed, so from the literature it can be said that it is a composite. Moreover, there is a slight shift in peaks that affirms good complexation, that is, the interaction of polymer with salt and ionic liquid.

4 | Performance of Supercapacitor

4.1 | Low Frequency Impedance Spectroscopy (LIS)

Low-frequency impedance spectroscopy is used to determine the specific capacitance by applying the formula:

$$C = -\frac{1}{\omega Z''} \quad (4)$$

$$C = -\frac{1}{2\pi f Z''} \quad (5)$$

We observed a maximum specific capacitance value of 124 Fg^{-1} using low-frequency data (Figure 10).

In general, the value of specific capacitance obtained from low-frequency impedance spectroscopy (LIS) can sometimes be underestimated when compared to other techniques like cyclic voltammetry (CV), and it is the only indication that the supercapacitor device is showing capacitive behavior. The actual values from the DC measurement, like CV, are discussed next.

4.2 | Cyclic Voltammetry (CV)

CV analysis was performed on polyether-derived carbon and solid polymer electrolyte-based cells. The analysis was conducted at various voltage ranges, starting from 0V and increasing to positive values (0–0.5V, 0–0.75V, 0–1V, 0–1.25V, 0–1.5V, 0–1.75V, and 0–2V), as shown in Figure 11a. Additionally, the analysis was also conducted at voltage ranges starting from negative to positive values (–0.5 to 0.5V, –0.75 to 0.75V, –1 to 1V, –1.25 to 1.25V, –1.5 to 1.5V, and –1.75 to 1.75V) as shown in Figure 11c. The scan rate used for the analysis was 10mVs^{–1}. In addition, the performance of supercapacitor cell was evaluated at several scan rates ranging from 5 to 100mVs^{–1} (5, 10, 20, 30, 40, 50, 70 and 100mVs^{–1}), with a potential range of 0 to 1.5V (Table 6, Figure 11b) and a potential range of –1.5 to 1.5V (Figure 11d).

The CV curves of the supercapacitor cell exhibited characteristic pseudo-type behavior, demonstrating excellent cyclic reversibility over the range of scan rates examined. Furthermore, throughout the extensive range of potential, the cell exhibited impressive stability and demonstrated excellent performance.

In addition to the cyclic behavior of supercapacitor cell, CV was employed to calculate the specific capacitance, which quantifies the total amount of charge that can be stored per unit mass of the material used as the electrode using the following equation:

$$C = \frac{i}{s} \quad (6)$$

The Equation (6) represents the relationship between specific capacitance (C), current (i), and scan rate (s).

The polyether carbon-based supercapacitor cell has the maximum specific capacitance of 228Fg^{–1} at a scan rate of 5mVs^{–1}, as shown in Table 8.

Furthermore, Tables 5 and 7 provide a summary of the specific capacitance of the polyether carbon-based supercapacitor cell at a scan rate of 10mVs^{–1} with various voltage ranges.

5 | Conclusion

Conducting solid polymer electrolyte (SPE) films comprising PVdF-HFP as precursor, NaSCN as salt and TBMPI as ionic liquid were prepared for the enhancement of ionic conductivity using solution casting technique. An improvement in ionic conductivity was noticed when an ionic liquid (IL) was added to the PVdF-HFP-based polymer matrix. The highest ionic conductivity value of 8.3 × 10^{–5} Scm^{–1} was achieved with a composition containing 150wt% of IL. The ionic transference number of mobile species in the optimized ion-conducting polymer

electrolyte, composed of PVdF-HFP + 40wt% NaSCN + 150wt% IL, was determined to be 0.95. This value is quite significantly higher than the electronic transference number, which is 0.05. LSV experiment revealed that the highly ion-conducting sample has a voltage window of 3.4V, finding it ideal for supercapacitor applications. Adding varying amounts of IL to the optimized PVdF-HFP:NaSCN polymer-salt combination altered the surface morphology of the SPE films as shown by POM. The complexation of the polymer, salt, and IL is confirmed by the significant shifts in the wavenumber of vibrational bands and a shift in the level of contact that appear in FT-IR spectra of IL-doped electrolyte films. The specific capacitance calculated with the cyclic voltammetry curve was found to be 228Fg^{–1} and relatively close value of 124Fg^{–1} was obtained at low frequency by impedance spectroscopy. These findings emphasize the significance of incorporating synthetic polymers in energy storage devices and the development of clean energies and technology.

Conflicts of Interest

The authors declare no conflicts of interest.

Data Availability Statement

The data that support the findings of this study are available from the corresponding author upon reasonable request.

References

1. L. Jeffry, M. Y. Ong, S. Nomanbhay, M. Mofijur, M. Mubashir, and P. L. Show, "Greenhouse Gases Utilization: A Review," *Fuel* 301 (2021): 121017, <https://doi.org/10.1016/j.fuel.2021.121017>.
2. S. R. Sinsel, R. L. Riemke, and V. H. Hoffmann, "Challenges and Solution Technologies for the Integration of Variable Renewable Energy Sources—A Review," *Renewable Energy* 145 (2020): 2271–2285, <https://doi.org/10.1016/j.renene.2019.06.147>.
3. T. M. Gür, "Review of Electrical Energy Storage Technologies, Materials and Systems: Challenges and Prospects for Large-Scale Grid Storage," *Energy & Environmental Science* 11, no. 10 (2018): 2696–2767, <https://doi.org/10.1039/C8EE01419A>.
4. A. G. Olabi, Q. Abbas, A. Al Makky, and M. A. Abdelkareem, "Supercapacitors as Next Generation Energy Storage Devices: Properties and Applications," *Energy* 248 (2022): 123617, <https://doi.org/10.1016/j.energy.2022.123617>.
5. P. Sharma and V. Kumar, "Current Technology of Supercapacitors: A Review," *Journal of Electronic Materials* 49, no. 6 (2020): 3520–3532, <https://doi.org/10.1007/s11664-020-07992-4>.
6. K. S. Poonam, A. Arora, and S. K. Tripathi, "Review of Supercapacitors: Materials and Devices," *Journal of Energy Storage* 21 (2019): 801–825, <https://doi.org/10.1016/j.est.2019.01.010>.
7. Q. Zhang and B. Wei, "Faradaic and Non-Faradaic Self-Discharge Mechanisms in Carbon-Based Electrochemical Capacitors," *Small* (2024): 2311957, <https://doi.org/10.1002/sml.202311957>.
8. K. K. Patel, T. Singhal, V. Pandey, T. P. Sumangala, and M. S. Sreekanth, "Evolution and Recent Developments of High Performance Electrode Material for Supercapacitors: A Review," *Journal of Energy Storage* 44 (2021): 103366, <https://doi.org/10.1016/j.est.2021.103366>.
9. S. B. Aziz, I. Brevik, M. H. Hamsan, et al., "Compatible Solid Polymer Electrolyte Based on Methyl Cellulose for Energy Storage Application: Structural, Electrical, and Electrochemical Properties," *Polymers* 12, no. 10 (2020): 2257, <https://doi.org/10.3390/polym12102257>.

10. S. Samantaray, D. Mohanty, I.-M. Hung, M. Moniruzzaman, and S. K. Satpathy, "Unleashing Recent Electrolyte Materials for Next-Generation Supercapacitor Applications: A Comprehensive Review," *Journal of Energy Storage* 72 (2023): 108352, <https://doi.org/10.1016/j.est.2023.108352>.
11. Y. An, X. Han, Y. Liu, et al., "Progress in Solid Polymer Electrolytes for Lithium-Ion Batteries and Beyond," *Small* 18, no. 3 (2022): 2103617, <https://doi.org/10.1002/smll.202103617>.
12. A. Dutta, S. Mitra, M. Basak, and T. Banerjee, "A Comprehensive Review on Batteries and Supercapacitors: Development and Challenges Since Their Inception," *Energy Storage* 5, no. 1 (2023): e339, <https://doi.org/10.1002/est2.339>.
13. S. Alipoori, S. Mazinani, S. H. Aboutalebi, and F. Sharif, "Review of PVA-Based Gel Polymer Electrolytes in Flexible Solid-State Supercapacitors: Opportunities and Challenges," *Journal of Energy Storage* 27 (2020): 101072, <https://doi.org/10.1016/j.est.2019.101072>.
14. T. A. Manfo, S. Konwar, P. K. Singh, R. M. Mehra, Y. Kumar, and M. Gupta, "PEO + NaSCN and Ionic Liquid Based Polymer Electrolyte for Supercapacitor," *Materials Today Proceedings* 34 (2021): 802–812, <https://doi.org/10.1016/j.matpr.2020.05.340>.
15. S. N. F. Yusuf, R. Yahya, and A. K. Arof, "Ionic Liquid Enhancement of Polymer Electrolyte Conductivity and Their Effects on the Performance of Electrochemical Devices," in *Progress and Developments in Ionic Liquids*, ed. S. Handy (InTech, 2017), <https://doi.org/10.5772/65752>.
16. N. S. Jishnu, S. K. Vineeth, A. Das, et al., "Electrospun PVdF and PVdF-co-HFP-Based Blend Polymer Electrolytes for Lithium Ion Batteries," in *Electrospinning for Advanced Energy Storage Applications. Materials Horizons: From Nature to Nanomaterials*, eds. N. T. M. Balakrishnan and R. Prasanth (Singapore: Springer Singapore, 2021), 201–234, https://doi.org/10.1007/978-981-15-8844-0_8.
17. M. Yang, B. Zhao, J. Li, et al., "Modified Poly(Vinylidene Fluoride-co-Hexafluoropropylene) Polymer Electrolyte for Enhanced Stability and Polymer Degradation Inhibition Toward the Li Metal Anode," *ACS Applied Energy Materials* 5, no. 7 (2022): 9049–9057, <https://doi.org/10.1021/acsaem.2c01505>.
18. S. Nazir, S. P. Pandey, F. A. Latif, and P. K. Singh, "Current Scenario and Future Prospective of Ionic-Liquid Doped Polymer Electrolyte for Energy Application," *Macromolecular Symposia* 413, no. 1 (2024): 2300035, <https://doi.org/10.1002/masy.202300035>.
19. M. J. Hussain, C. S. Espenti, Y. V. M. Reddy, P. Saraswathi, J. P. Park, and G. Madhavi, "Investigation of the Electrochemical Performance of Mg-Ion Batteries Based on PVDF-HFP Thin Polymer Electrolyte Films," *Materials Chemistry and Physics* 313 (2024): 128745, <https://doi.org/10.1016/j.matchemphys.2023.128745>.
20. Z. Wang, M. Zhu, Z. Pei, et al., "Polymers for Supercapacitors: Boosting the Development of the Flexible and Wearable Energy Storage," *Materials Science and Engineering: R: Reports* 139 (2020): 100520, <https://doi.org/10.1016/j.mser.2019.100520>.
21. P. S. Dhapola, M. Karakoti, S. Kumar, et al., "Environment-Friendly Approach for Synthesis of Promising Porous Carbon: Empowering Supercapacitors for a Sustainable Future," *Materials Advances* 5, no. 6 (2024): 2430–2440, <https://doi.org/10.1039/D3MA00984J>.
22. S. Kumar, P. K. Singh, V. D. Punetha, et al., "In-Situ N/O-Heteroatom Enriched Micro-/Mesoporous Activated Carbon Derived From Natural Waste Honeycomb and Paper Wasp Hive and Its Application in Quasi-Solid-State Supercapacitor," *Journal of Energy Storage* 72 (2023): 108722, <https://doi.org/10.1016/j.est.2023.108722>.
23. M. Karakoti, R. Jangra, S. Pandey, et al., "Binder-Free Reduced Graphene Oxide as Electrode Material for Efficient Supercapacitor With Aqueous and Polymer Electrolytes," *High Performance Polymers* 32, no. 2 (2020): 175–182, <https://doi.org/10.1177/0954008320905659>.
24. H. Gudla, Y. Shao, S. Phunnarungsi, D. Brandell, and C. Zhang, "Importance of the Ion-Pair Lifetime in Polymer Electrolytes," *Journal of Physical Chemistry Letters* 12, no. 35 (2021): 8460–8464, <https://doi.org/10.1021/acs.jpclett.1c02474>.
25. A. T. Manfo, P. K. Singh, R. M. Mehra, R. C. Singh, and M. Gupta, "Structural, Vibrational, Electrical, Electrochemical and Capacitive Investigations on Ionic Liquid Doped P (VDF-HFP) + NaSCN Based Polymer Electrolytes," *Rice* 14, no. 1 (2021): 21–34, <https://doi.org/10.2174/2405520413999200719141337>.
26. A. L. Ahmad, U. R. Farooqui, and N. A. Hamid, "Porous (PVDF-HFP/PANI/GO) Ternary Hybrid Polymer Electrolyte Membranes for Lithium-Ion Batteries," *RSC Advances* 8, no. 45 (2018): 25725–25733, <https://doi.org/10.1039/C8RA03918F>.
27. S. Rajendran, O. Mahendran, and R. Kannan, "Lithium ion Conduction in Plasticized PMMA–PVdF Polymer Blend Electrolytes," *Materials Chemistry and Physics* 74, no. 1 (2002): 52–57, [https://doi.org/10.1016/S0254-0584\(01\)00400-X](https://doi.org/10.1016/S0254-0584(01)00400-X).
28. K. Karpagavel, K. Sundaramahalingam, A. Manikandan, et al., "Electrical Properties of Lithium-Ion Conducting Poly (Vinylidene Fluoride-co-Hexafluoropropylene) (PVDF-HFP)/Polyvinylpyrrolidone (PVP) Solid Polymer Electrolyte," *Journal of Electronic Materials* 50, no. 8 (2021): 4415–4425, <https://doi.org/10.1007/s11664-021-08967-9>.
29. S. Badatya, A. Kumar, C. Sharma, A. K. Srivastava, J. P. Chaurasia, and M. K. Gupta, "Transparent Flexible Graphene Quantum Dot-(PVDF-HFP) Piezoelectric Nanogenerator," *Materials Letters* 290 (2021): 129493, <https://doi.org/10.1016/j.matlet.2021.129493>.
30. P. Huang, S. Xu, W. Zhong, et al., "Carbon Quantum Dots Inducing Formation of β Phase in PVDF-HFP to Improve the Piezoelectric Performance," *Sensors and Actuators A: Physical* 330 (2021): 112880, <https://doi.org/10.1016/j.sna.2021.112880>.
31. N. Ataollahi, A. Ahmad, H. Hamzah, M. Y. A. Rahman, and N. S. Mohamed, "Preparation and Characterization of PVDF-HFP/MG49 Based Polymer Blend Electrolyte," *International Journal of Electrochemical Science* 7, no. 8 (2012): 6693–6703, [https://doi.org/10.1016/S1452-3981\(23\)15740-3](https://doi.org/10.1016/S1452-3981(23)15740-3).
32. P. Tuhania, P. K. Singh, B. Bhattacharya, et al., "PVDF-HFP and 1-Ethyl-3-Methylimidazolium Thiocyanate-Doped Polymer Electrolyte for Efficient Supercapacitors," *High Performance Polymers* 30, no. 8 (2018): 911–917, <https://doi.org/10.1177/0954008318772009>.
33. P. Bernardo, D. Zampino, and G. Clarizia, "Triggering the Gas Transport in PVdF-HFP Membranes via Imidazolium Ionic Liquids," *Separation and Purification Technology* 250 (2020): 117201, <https://doi.org/10.1016/j.seppur.2020.117201>.
34. A. L. Ahmad, U. R. Farooqui, and N. A. Hamid, "Effect of Graphene Oxide (GO) on Poly(Vinylidene Fluoride-Hexafluoropropylene) (PVDF-HFP) Polymer Electrolyte Membrane," *Polymer* 142 (2018): 330–336, <https://doi.org/10.1016/j.polymer.2018.03.052>.
35. C.-C. Yang, Y.-C. Chen, Z.-Y. Lian, T.-H. Liou, and J.-Y. Shih, "Fabrication and Characterization of P(VDF-HFP)/SBA-15 Composite Membranes for Li-Ion Batteries," *Journal of Solid State Electrochemistry* 16, no. 5 (2012): 1815–1821, <https://doi.org/10.1007/s10008-011-1574-6>.
36. H. Manjunatha, R. Damle, and G. N. Kumaraswamy, "Modification of Polymer Electrolyte Blend PEO/PVDF-HFP by Low-Energy O⁺ Ion Irradiation to Improve Electrolyte Behavior," *Polymer Bulletin* 79, no. 6 (2022): 3929–3950, <https://doi.org/10.1007/s00289-021-03693-y>.
37. A. L. Ahmad, U. R. Farooqui, and N. A. Hamid, "Synthesis and Characterization of Porous Poly(Vinylidene Fluoride-co-Hexafluoropropylene) (PVDF-co-HFP)/Poly(Aniline) (PANI)/Graphene Oxide (GO) Ternary Hybrid Polymer Electrolyte Membrane," *Electrochimica Acta* 283 (2018): 842–849, <https://doi.org/10.1016/j.electacta.2018.07.001>.
38. H. Parangusan, D. Ponnamma, and M. A. A. Al-Maadeed, "Stretchable Electrospun PVDF-HFP/co-ZnO Nanofibers as Piezoelectric Nanogenerators," *Scientific Reports* 8, no. 1 (2018): 754, <https://doi.org/10.1038/s41598-017-19082-3>.

39. A. N. Alias, Z. M. Zabidi, M. K. Harun, M. Z. A. Yahya, and A. M. M. Ali, "Optical Transition, Excitation, and Emission Properties of Poly(N-Vinylcarbazole) Blended With Poly(Vinylidene Fluoride-co-Hexafluoropropene) and Polyvinylpyrrolidone," *Acta Physica Polonica A* 127, no. 4 (2015): 1075–1078, <https://doi.org/10.12693/APhysPolA.127.1075>.
40. X. Zhao, C. Wang, H. Liu, Y. Liang, and L. Fan, "A Review of Polymer-Based Solid-State Electrolytes for Lithium-Metal Batteries: Structure, Kinetic, Interface Stability, and Application," *Batteries & Supercaps* 6, no. 4 (2023): e202200502, <https://doi.org/10.1002/batt.202200502>.
41. L. Fernandes, R. Meira, D. Correia, et al., "Electrospun Magnetic Ionic Liquid Based Electroactive Materials for Tissue Engineering Applications," *Nanomaterials* 12, no. 17 (2022): 3072, <https://doi.org/10.3390/nano12173072>.
42. X. Hao, H. Wenren, X. Wang, X. Xia, and J. Tu, "A Gel Polymer Electrolyte Based on PVDF-HFP Modified Double Polymer Matrices via Ultraviolet Polymerization for Lithium-Sulfur Batteries," *Journal of Colloid and Interface Science* 558 (2020): 145–154, <https://doi.org/10.1016/j.jcis.2019.09.116>.
43. H. Gao, W. Zhou, K. Park, and J. B. Goodenough, "A Sodium-Ion Battery With a Low-Cost Cross-Linked Gel-Polymer Electrolyte," *Advanced Energy Materials* 6, no. 18 (2016): 1600467, <https://doi.org/10.1002/aenm.201600467>.
44. H. Li, C. Chao, P. Han, X. Yan, and H. Zhang, "Preparation and Properties of Gel-Filled PVDF Separators for Lithium Ion Cells," *Journal of Applied Polymer Science* 134, no. 7 (2017): 6–11, <https://doi.org/10.1002/app.44473>.
45. P. Tamilarasan and S. Ramaprabhu, "Graphene Based All-Solid-State Supercapacitors With Ionic Liquid Incorporated Polyacrylonitrile Electrolyte," *Energy* 51 (2013): 374–381, <https://doi.org/10.1016/j.energy.2012.11.037>.
46. S. Bhattacharya, R. Manojkumar Ubarhande, M. Usha Rani, R. Shanker Babu, and R. Arunkumar, "TiO₂ as Conductivity Enhancer in PVdF-HFP Polymer Electrolyte System," *IOP Conference Series: Materials Science and Engineering* 263 (2017): 022006, <https://doi.org/10.1088/1757-899X/263/2/022006>.
47. B. Halder and P. Elumalai, "Composite Polymer Electrolyte Facilitated by Enhanced Amorphousness and Li⁺ Conduction Using LaFeO₃-Embedded PVDF-HFP for Solid-State Lithium Metal Battery," *Journal of Colloid and Interface Science* 669 (2024): 992–1005, <https://doi.org/10.1016/j.jcis.2024.05.071>.
48. D. M. Correia, C. M. Costa, J. C. Rodríguez Hernández, et al., "Crystallization Monitoring of Semicrystalline Poly(Vinylidene Fluoride)/1-Ethyl-3-Methylimidazolium Hexafluorophosphate [Emim][PF₆] Ionic Liquid Blends," *Crystal Growth & Design* 21, no. 8 (2021): 4406–4416, <https://doi.org/10.1021/acs.cgd.1c00333>.
49. J. Lee, J. Yoon, J. Jeon, Y. Hong, S.-G. Oh, and H. Huh, "Electrospun PVDF-HFP/PAN Bicomponent Nanofibers as Separators in Lithium-Ion Batteries With High Thermal Stability and Electrolyte Wettability," *Korean Journal of Chemical Engineering* 40, no. 8 (2023): 1901–1911, <https://doi.org/10.1007/s11814-023-1486-z>.
50. M. K. Vyas and A. Chandra, "Ion-Electron-Conducting Polymer Composites: Promising Electromagnetic Interference Shielding Material," *ACS Applied Materials & Interfaces* 8, no. 28 (2016): 18450–18461, <https://doi.org/10.1021/acsami.6b05313>.
51. M. I. Diana, P. C. Selvin, S. Selvasekarapandian, and M. V. Krishna, "Investigations on Na-Ion Conducting Electrolyte Based on Sodium Alginate Biopolymer for All-Solid-State Sodium-Ion Batteries," *Journal of Solid State Electrochemistry* 25, no. 7 (2021): 2009–2020, <https://doi.org/10.1007/s10008-021-04985-z>.
52. N. Angulakshmi, S. Thomas, K. S. Nahm, A. M. Stephan, and R. N. Elizabeth, "Electrochemical and Mechanical Properties of Nanochitin-Incorporated PVDF-HFP-Based Polymer Electrolytes for Lithium Batteries," *Ionics* 17, no. 5 (2011): 407–414, <https://doi.org/10.1007/s11581-010-0517-z>.
53. P. Prabakaran, R. P. Manimuthu, S. Gurusamy, and E. Sebasthiyan, "Plasticized Polymer Electrolyte Membranes Based on PEO/PVdF-HFP for Use as an Effective Electrolyte in Lithium-Ion Batteries," *Chinese Journal of Polymer Science* 35, no. 3 (2017): 407–421, <https://doi.org/10.1007/s10118-017-1906-9>.
54. X. Huang, X. Gao, X. Wang, H. Shang, and S. Zhou, "Multifunctional Superamphiphobic Coating Based on Fluorinated TiO₂ Toward Effective Anti-Corrosion," *Materials* 17, no. 10 (2024): 2203, <https://doi.org/10.3390/ma17102203>.
55. N. Kundana, M. Venkatapathy, V. N. V. Neeraja, C. S. Espenti, V. M. Reddy, and V. Jeedi, "Effect of PMMA on PVDF-Co-HFP/MgTf₃ Polymer Composite With Improved Ionic Conductivity, Thermal and Structural Properties," *Oriental Journal of Chemistry* 38, no. 5 (2022): 1138–1147, <https://doi.org/10.13005/ojc/380508>.
56. W. Z. N. Yahya, W. T. Meng, M. Khatani, A. E. Samsudin, and N. M. Mohamed, "Bio-Based Chitosan/PVdF-HFP Polymer-Blend for Quasi-Solid State Electrolyte Dye-Sensitized Solar Cells," *E-Polymers* 17, no. 5 (2017): 355–361, <https://doi.org/10.1515/epoly-2016-0305>.
57. M. Sasikumar, A. Jagadeesan, M. Raja, R. Hari Krishna, and P. Sivakumar, "The Effects of PVAc on Surface Morphological and Electrochemical Performance of P(VdF-HFP)-Based Blend Solid Polymer Electrolytes for Lithium Ion-Battery Applications," *Ionics* 25, no. 5 (2019): 2171–2181, <https://doi.org/10.1007/s11581-018-2679-z>.
58. T. M. W. J. Bandara, A. M. J. S. Weerasinghe, M. A. K. L. Dissanayake, et al., "Characterization of Poly (Vinylidene Fluoride-Co-Hexafluoropropylene) (PVdF-HFP) Nanofiber Membrane Based Quasi Solid Electrolytes and Their Application in a Dye Sensitized Solar Cell," *Electrochimica Acta* 266 (2018): 276–283, <https://doi.org/10.1016/j.electacta.2018.02.025>.
59. L. Yesappa, S. P. Ashokkumar, H. Vijeth, M. Basappa, S. Ganesh, and H. Devendrappa, "Effect of Electron Beam Irradiation on Structure, Morphology, and Optical Properties of PVDF-HFP/PEO Blend Polymer Electrolyte Films," *Journal of Radioanalytical and Nuclear Chemistry* 322, no. 1 (2019): 5–10, <https://doi.org/10.1007/s10967-019-06466-0>.
60. K. Yang, X. Ma, K. Sun, Y. Liu, and F. Chen, "Electrospun Octa(3-Chloropropyl)-polyhedral Oligomeric Silsesquioxane-Modified Polyvinylidene Fluoride/Poly(Acrylonitrile)/Poly(Methylmethacrylate) Gel Polymer Electrolyte for High-Performance Lithium Ion Battery," *Journal of Solid State Electrochemistry* 22, no. 2 (2018): 441–452, <https://doi.org/10.1007/s10008-017-3758-1>.
61. S. K. Chacko, M. T. Rahul, B. Raneesh, K. Vinodan, J. K. Jose, and N. Kalarikkal, "Enhanced Electroactive Phase, Dielectric Properties and Tuning of Bandgap in Ho³⁺ Modified PVDF-HFP Composite Films," *Journal of Polymer Research* 29, no. 11 (2022): 493, <https://doi.org/10.1007/s10965-022-03318-6>.
62. L. N. Sim, S. R. Majid, and A. K. Arof, "FTIR Studies of PEMA/PVdF-HFP Blend Polymer Electrolyte System Incorporated With LiCF₃SO₃ Salt," *Vibrational Spectroscopy* 58 (2012): 57–66, <https://doi.org/10.1016/j.vibspec.2011.11.005>.
63. A. Mallikarjun, J. S. Kumar, T. Sreekanth, et al., "Investigation of FT-IR and Impedance Spectroscopy of Nanocomposite PVDF-HFP Based Polymer Electrolytes," *Materials Today Proceedings* (2023): S2214785323002791, <https://doi.org/10.1016/j.matpr.2023.01.215>.
64. C.-C. Yang, Z.-Y. Lian, S. J. Lin, J.-Y. Shih, and W.-H. Chen, "Preparation and Application of PVDF-HFP Composite Polymer Electrolytes in LiNi_{0.5}Co_{0.2}Mn_{0.3}O₂ Lithium-Polymer Batteries," *Electrochimica Acta* 134 (2014): 258–265, <https://doi.org/10.1016/j.electacta.2014.04.100>.
65. D. Ponnamma, O. Aljarod, H. Parangusan, and M. A. Ali Al-Maadeed, "Electrospun Nanofibers of PVDF-HFP Composites

Containing Magnetic Nickel Ferrite for Energy Harvesting Application," *Materials Chemistry and Physics* 239 (2020): 122257, <https://doi.org/10.1016/j.matchemphys.2019.122257>.

66. S. A. Mohd Noor, C. P. Wong, M. Z. Dzulklipli, M. S. Su'ait, L. T. Khoo, and N. H. Hassan, "Properties of Gel Polymer Electrolyte Based Poly(Vinylidene Fluoride-co-Hexafluoropropylene) (PVdF-HFP), Lithium Perchlorate (LiClO_4) and 1-Butyl-3-Methylimidazoliumhexafluorophosphate [PF_6]," *Solid State Phenomena* 317 (2021): 434–439, <https://doi.org/10.4028/www.scientific.net/SSP.317.434>.